Overmodulation Techniques of Asymmetrical Six-phase Machine With Optimum Harmonic Voltage Injection

Sayan Paul, Kaushik Basu, *Senior Member, IEEE*

***Abstract*—Overmodulation techniques of asymmetrical six-phase machine achieve higher DC-bus utilization by applying voltage in non-energy transfer plane. This results into unwanted current and associated copper loss. Existing overmodulation technique minimizes this voltage from space-vector perspective with pre-defined set of four active vectors. To find the best technique, one needs to perform the above minimization problem with all possible sets of active vectors with which higher voltage gain can be attained. So, this requires evaluation of large number of cases. This paper formulates the above minimization problem in terms of average voltage vectors of two three-phase inverters, where active vectors need not to be specified beforehand and thus the analysis is more general. Sixteen possible techniques with different set of active vectors are derived following the above analysis, which attain minimum voltage injection in non-energy transfer plane. This paper also identifies one of these sixteen techniques, which can be implemented without involving complex six-dimensional transformation. The above technique is validated through experiments on six-phase induction motor and simulations in Matlab at 3.5 kW power level.**

***Index Terms*—Multiphase machines, pulse width modulation (PWM), overmodulation, asymmetrical six-phase induction motor, six-phase drives, harmonic minimization.**

NOMENCLATURE

$\overline{x}$	Switching cycle average of variable x
$\overline{v}_{\underline{\alpha}} + j\overline{v}_{\beta}$	3ϕ average voltage space-vector of Inverter-1.
$\overline{v'}_{\underline{\alpha}} + j\overline{v'}_{\beta}$	3ϕ average voltage space-vector of Inverter-2.
$\overline{v}_{\alpha} + j\overline{v}_{\beta}$	6ϕ average voltage space-vector in $\alpha-\beta$ plane.
$\overline{v}_{z_1} + j\overline{v}_{z_2}$	6ϕ average voltage space-vector in $z_1 - z_2$.
$\vec{V}_{ref}$	Reference voltage vector in $\alpha - \beta$
M	Modulation index

I. INTRODUCTION

ASYMMETRICAL six-phase machine (ASPM), one of the most popular multi-phase machines, has two sets of balanced three-phase (3ϕ) windings which are spatially shifted by 30° electrical, as shown in Fig. 1. This machine is attractive in high power applications compared to 3ϕ due to better fault tolerance for having more number of phases, reduced rating of per-phase power-electronic drive unit, less susceptibility towards excitation harmonics, [1], [2].

Manuscript received December 13, 2019; revised March 28, 2020; accepted April 06, 2020. This work was supported by Department of Science and Technology, Government of India under the project titled "Development of an advanced System-On-Chip (SoC) based embedded controller for power electronic converters". (Corresponding author : Sayan Paul).

The authors are with the Department of Electrical Engineering, Indian Institute of Science, Bangalore 560012, India. (e-mail: sayanp@iisc.ac.in; kbasu@iisc.ac.in).

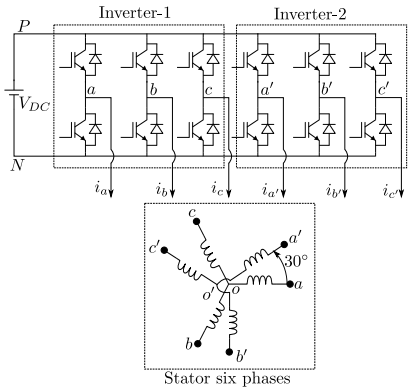

Fig. 1: Six-phase inverter fed ASPM

To model ASPM with sinusoidal winding distribution, [3] proposed a 6×6 orthonormal transformation matrix, T. T transforms the six-dimensional quantities from original frame to three two-dimensional orthogonal subspaces, as $\alpha - \beta$, $z_1 - z_2$ and $o_1 - o_2$, and the dynamic models of ASPM are decoupled in these subspaces. $\alpha - \beta$ subspace is associated with electromechanical energy transfer and therefore, this subspace should be excited with balanced fundamental voltage in order to generate ripple-free torque in ASPM. The air-gap flux doesn't appear in other subspaces and hence torque remains unaffected with the applied voltages in these subspaces. With the balanced winding with two isolated neutrals, as shown in Fig. 1, $o_1 - o_2$ plane can't be excited. Although applied voltage in $z_1 - z_2$ doesn't create torque pulsation, it causes large circulating current and associated copper loss due to low impedance of the equivalent circuit. Therefore, applied voltage in $z_1 - z_2$ should be as minimum as possible.

Linear modulation techniques of six-phase (6ϕ) inverter fed ASPM don't apply any average voltage in $z_1 - z_2$ subspace. These techniques can be broadly classified into two categories: space-vector based techniques (SVPWM) and two-inverter (TINV) based techniques. In SVPWM techniques, desired voltages in $\alpha-\beta$ and zero voltages in z_1-z_2 are synthesised by the application of at least four active vectors and zero vectors. SVPWM based linear modulation techniques with different choice and number of active vectors and their performance comparisons are presented in [3]–[10]. To avoid complex implementation strategy of SVPWM based techniques, [11], [12] modulate two 3ϕ inverters with reference voltage vectors of equal magnitude at a phase difference of 30°. The resulting

techniques don't apply any voltage in $z_1 - z_2$ subspace. These are labelled as TINV techniques in this paper. If modulation index (M) is defined as the ratio of peak of fundamental line-neutral voltage and DC-bus voltage, the maximum M attainable by both of these categories is 0.577.

Overmodulation (OVM) techniques apply a group of harmonics in line-neutral voltages to attain $0.577 < M \leq 0.622$ so that these harmonics appear only in $z_1 - z_2$ without affecting fundamental operation in $\alpha - \beta$. [13] proposed one such technique, which is known as *CSVPWM* ([3]), where desired voltage vector in $\alpha - \beta$ was synthesised using two adjacent active vectors. This resulted into large circulating current in $z_1 - z_2$ plane, [3]. To minimize this, [6] had proposed two space-vector based OVM (SVOVM) techniques, named as *SVOVM4-1* and *SVOVM4-2* in this paper, which use two pairs of active vectors adjacent to the reference voltage vector in $\alpha - \beta$ without any zero-vector. Each pair consists of largest and medium collinear vectors of $\alpha - \beta$. With these vectors, *SVOVM4-2* formulated an optimization problem to achieve minimum RMS voltage in $z_1 - z_2$ and it is the best known technique among all existing OVM techniques of ASPM. It should be mentioned here that OVM of symmetrical five-phase machine with one isolated neutral also requires four-dimensional modulation like ASPM, [14]–[18]. [14], [15] proposed OVM technique of five-phase machine using similar pairs of voltage vectors as [6]. [19] proposed TINV based OVM techniques in which two 3ϕ inverters were operated through OVM schemes of 3ϕ inverters, as proposed by [20], in 30° phase difference. But, these techniques resulted into injection of harmonics in $\alpha - \beta$.

In SVPWM based voltage minimization technique, like *SVOVM4-2* of [6], the active vectors need to be decided beforehand. As there are multiple ways of choosing these active vectors, one needs to perform the minimization problem for all such choices to find the best technique. In this context, this paper makes following three contributions.

- The average voltage space-vectors of 6ϕ inverter in $\alpha - \beta$ and $z_1 - z_2$ planes are expressed in terms of average voltage space-vectors of two 3ϕ inverters. Then, the aforementioned voltage minimization in $z_1 - z_2$ is formulated in terms of these 3ϕ average voltage vectors. Thus, the problem formulation doesn't require specification of the active vectors beforehand and the analysis is more general.
- Based on the above analysis, the whole OVM region is divided into two parts. Optimal solution can be realized by eight possible sets of switching states in one part and two possible sets in another part. Combining these two, sixteen possible techniques are obtained to attain optimal solution. *SVOVM4-2* is one such technique.
- Finally, this paper presents a two-inverter based optimal OVM technique which can be implemented without involving complex 6ϕ transformation and only requires knowledge of 3ϕ inverter modulation.

The organization of the paper is as follows. Section II briefly describe the modeling of 6ϕ machine and converter and existing space-vector based OVM techniques. Section III formulates the optimization problem to attain global minimum voltage injection in $z_1 - z_2$ plane and section IV derives few SVOVM techniques to attain this global minima. Finally, carrier based implementation of one of the SVOVM techniques with optimum harmonic voltage injection is discussed in section-V and validated through experiments and simulations in section VI. The paper has been concluded in section VII.

II. Existing Overmodulation techniques of Asymmetrical Six-phase Machine

Fig. 1 shows the connection diagram of six stator phases of asymmetrical six-phase machine (ASPM) with two-level 6ϕ inverter. *The 6ϕ inverter can be viewed as two 3ϕ inverters, inverter-1 and inverter-2.* The terminals of the six stator phase windings are a, b, c, a', b', c', which are directly connected to the poles of the six legs of the inverter. These two sets of balanced 3ϕ windings are connected in star fashion with two isolated neutral points, o and o', and these two sets are spatially shifted by 30°.

A. Machine Modeling

$$X_i \triangleq \underbrace{\frac{1}{\sqrt{3}} \begin{bmatrix} 1 & -\frac{1}{2} & -\frac{1}{2} & \frac{\sqrt{3}}{2} & -\frac{\sqrt{3}}{2} & 0 \\ 0 & \frac{\sqrt{3}}{2} & -\frac{\sqrt{3}}{2} & \frac{1}{2} & \frac{1}{2} & -1 \\ 1 & -\frac{1}{2} & -\frac{1}{2} & -\frac{\sqrt{3}}{2} & \frac{\sqrt{3}}{2} & 0 \\ 0 & -\frac{\sqrt{3}}{2} & \frac{\sqrt{3}}{2} & \frac{1}{2} & \frac{1}{2} & -1 \\ 1 & 1 & 1 & 0 & 0 & 0 \\ 0 & 0 & 0 & 1 & 1 & 1 \end{bmatrix}}_{T} X_j$$

$$X_i = \begin{bmatrix} x_\alpha & x_\beta & x_{z_1} & x_{z_2} & x_{o_1} & x_{o_2} \end{bmatrix}^T$$
$$X_j = \begin{bmatrix} x_a & x_b & x_c & x_{a'} & x_{b'} & x_{c'} \end{bmatrix}^T \quad (1)$$

[3] has proposed a 6×6 orthonormal transformation matrix T, as given in (1), to analyse the dynamic model of ASPM in transformed domain, $\alpha - \beta - z_1 - z_2 - o_1 - o_2$. The vector quantities in (1) can be voltage, current or flux-linkage etc. . Followings are few important properties of ASPM in transformed domain.

1) The transformed six dimensions are orthogonal to each other and can be grouped as three two-dimensional subspaces, viz., $\alpha - \beta$, $z_1 - z_2$ and $o_1 - o_2$, respectively. Dynamic equivalent circuits of ASPM in these subspaces are decoupled to each other.
2) The coupling of flux-linkages and currents between stator and rotor is seen only in $\alpha - \beta$ subspace. Both the dynamical and steady-state equivalent circuits in this subspace are similar to the equivalent circuits of 3ϕ machine with 3ϕ Clarke's transformation. This is the only subspace associated with electromechanical energy transfer and hence $\alpha - \beta$ plane should be excited with balanced fundamental voltage so as to rotate the ASPM without any torque ripple.
3) The dynamic and steady-state equivalent circuits in $z_1 - z_2$ and $o_1 - o_2$ subspaces consist of winding resistance and leakage inductance. These subspaces are not associated with electromechanical energy transfer. Although these subspaces don't create any torque pulsation, injection of

TABLE I: Switching States of Three-phase Inverter

Switching State	Label	Switching State	Label
000	0	011	4
100	1	001	5
110	2	101	6
010	3	111	7

voltages in these subspaces should be low to reduce the RMS current and associated loss in these subspaces. For two isolated neutrals (as shown in Fig. 1), i_{o_1}, i_{o_2} in (1), corresponding to line currents, are zero. So, v_{o_1}, v_{o_2}, corresponding to line-neutral voltages, for balanced six-phase windings will be always zero for any of the switching states of the inverter. Therefore, discussion of modulation in $o_1 - o_2$ subspace is omitted in subsequent sections.

B. Converter Modeling

As each of the two-level 3ϕ inverters has 8 permissible switching states, 6ϕ inverter of Fig. 1 has $8\times8 = 64$ switching states. These states are labelled by using two numbers, like (x, y'), where x, y' denote the switching states of inverter-1 and inverter-2, respectively, and $x, y \in \{0, 1...7\}$. Table I lists 8 switching states of 3ϕ inverter. Each entry under 'Switching State' column has three binary digits which denote the switching states of top switches of a, b, and c legs, respectively, of a 3ϕ inverter. Here, 0 represents 'off' and 1 represents 'on'. The bottom switch of any leg is complementary switched with respect to top switch. Therefore, 101 state implies top switches of a and c legs and bottom switch of b legs are in 'on' state. So, switching state $(1, 6')$ of 6ϕ inverter means top switches of a, a', c' and bottom switches of b, c, b' are 'on'; other switches are 'off'.

The line-neutral voltages generated by each of the switching states can be mapped into transformed domain by applying T of (1). For example, line-neutral voltage vector in original domain, V_j in (1), generated by state $(1, 6')$ is given as, $V_j|_{(1,6')} = \frac{V_{DC}}{3}\begin{bmatrix} 2 & -1 & -1 & 1 & -2 & 1 \end{bmatrix}^T$. The corresponding mapping in transformed domain, V_i, is obtained by applying T on V_j. Combining $\alpha - \beta$ and $z_1 - z_2$ voltages together, we get, $(v_\alpha + jv_\beta)|_{(1,6')} = \frac{2V_{DC}\cos 15^\circ}{\sqrt{3}}e^{-j15^\circ}$ and $(v_{z_1} + jv_{z_2})|_{(1,6')} = \frac{2V_{DC}\cos 75^\circ}{\sqrt{3}}e^{-j75^\circ}$. Similarly, 64 states can be mapped in transformed domain. It gives 60 active vectors (48 distinct vectors) and 4 zero vectors in both $\alpha - \beta$ and $z_1 - z_2$. The mapping of these 64 states can be referred from [3]. The tips of 12 largest active vectors in $\alpha - \beta$ form a do-decagon. $\alpha - \beta$ plane within this do-decagon can be divided in 12 equivalent sectors. Fig. 2 shows the mapping of those 16 states in $\alpha - \beta$ and $z_1 - z_2$ which are required to explain the space-vector based overmodulation (OVM) techniques with reference voltage vector, $\vec{V}_{ref}$, within sector-1 of $\alpha - \beta$ plane. $\vec{V}_{ref}$ is defined as $\vec{V}_{ref} \triangleq \overline{v}_\alpha + j\overline{v}_\beta$; bar represents the average value over a switching cycle. Among these 16 states, 4 are zero states and they are denoted by (z, z'), where $z \in \{0, 7\}$. Remaining 12 states give 9 distinct active vectors, shown in Fig. 2, as two zero states of one 3ϕ inverter in combination with one active state of other 3ϕ inverter give rise to same vector in both $\alpha - \beta$ and $z_1 - z_2$ planes. Therefore, each of the active vectors among $(z, 1')$, $(1, z')$ and $(z, 6')$ in Fig. 2

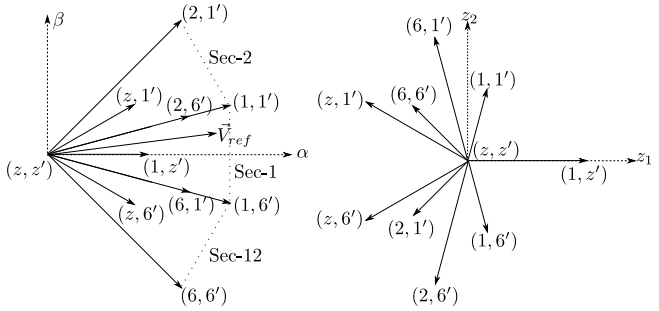

(a) $\alpha - \beta$ plane (b) $z_1 - z_2$ plane

Fig. 2: Mapping of 16 neighbouring switching states of sector-1 results into 10 distinct vectors

is the resultant of two states. The boundary of the do-decagon is shown by the dotted line in Fig. 2a and 12^{th}, 1^{st} and 2^{nd} sectors are indicated in the figure.

In this paper, modulation index (M) is defined as the ratio of peak of the fundamental line-neutral voltage and DC-bus voltage. *OVM techniques are referred to those techniques which don't apply any harmonic voltage in $\alpha - \beta$ but do apply harmonic voltages in $z_1 - z_2$ plane in order to achieve higher M*. It is well-known in ASPM literature that linear techniques attain M up to 0.577 whereas OVM techniques can achieve M up to 0.622. What follows is the brief discussion on existing OVM techniques of ASPM and their limitations.

C. Existing SVOVM techniques of ASPM and its limitations

Suppose, we want to synthesize $\vec{V}_{ref}$ in sector-1 of $\alpha - \beta$ plane, as shown in Fig. 2. Existing two-vector based SVOVM technique of [13], later named as *CSVPWM* in [3], *uses two large active vectors adjacent to $\vec{V}_{ref}$, like $(1, 6')$, $(1, 1')$ and zero-vector. Harmonic voltage injected by CSVPWM in $z_1 - z_2$ plane is significant, [3].* [6] has proposed two OVM techniques, which are termed as *SVOVM4-1* (space-vector based OVM technique using 4 active vectors) and *SVOVM4-2* in this paper, in order to reduce harmonic voltage injection in $z_1 - z_2$ plane. *It uses 2 large and 2 medium vectors adjacent to $\vec{V}_{ref}$, like $(6, 1')$, $(1, 6')$, $(2, 6')$ and $(1, 1')$ in sector-1.* With this four vectors, *SVOVM4-2 minimizes average voltage injected in $z_1 - z_2$ plane, $\overline{v}_{z_1}^2 + \overline{v}_{z_2}^2$*. Similar OVM techniques for five-phase drives were proposed by [14]–[16]. Suppose, the minimal voltage injection in $z_1 - z_2$ plane obtained by *SVOVM4-2* is denoted as $|\overline{v}_{z_1} + j\overline{v}_{z_2}|^*_{2L+2M}$.

Let us consider an *alternative 4 vector strategy*, that applies *2 large, 1 medium and 1 small* vectors adjacent to $\vec{V}_{ref}$ in sector-1 of $\alpha - \beta$ plane: $(1, z')$, $(1, 1')$, $(1, 6')$ and $(2, 6')$. For this particular choice of vectors, we can find the optimal modulation strategy following the similar analysis as outlined in [6] and suppose the optimal voltage is denoted by $|\overline{v}_{z_1} + j\overline{v}_{z_2}|^*_{2L+1M+1S}$. *We observed that $|\overline{v}_{z_1} + j\overline{v}_{z_2}|^*_{2L+1M+1S} \geq |\overline{v}_{z_1} + j\overline{v}_{z_2}|^*_{2L+2M}$ for all possible $\vec{V}_{ref}$ in overmodulation region of upper-half of sector-1*. But, if $(z, 1')$ is used instead of $(1, z')$ (where both $(z, 1')$ and $(1, z')$ are small vectors adjacent to $\vec{V}_{ref}$ in sector-1) keeping other three vectors

same, the optimal solution obtained by that set is same as $|\overline{v}_{z_1} + j\overline{v}_{z_2}|^*_{2L+2M}$.

The above example clearly establishes following facts: 1) There are more than one set of vectors that can be used to synthesize a reference voltage vector in $\alpha - \beta$ plane in overmodulation. 2) Following the procedure outlined in [6], one can find the duty ratios of this specific set of vectors that will minimize the length of the average applied vector in $z_1 - z_2$ plane 3) This minimum length depends on the choice of the set of vectors. So, *for a given reference voltage vector in overmodulation region, unless we compute the minimum lengths of the average voltage vectors in $z_1 - z_2$ plane by every possible techniques, we do not know a) SVOVM4-2 in [6] is the technique that attains smallest among all minimum lengths of the average voltage vectors in $z_1 - z_2$ plane (we can call it global minimum), b) even if that is true, are there techniques other than SVOVM4-2 in [6] that also achieves the same global minimum*. In order to find the best strategy, one needs to do the following: a) Determine all possible sets of adjacent vectors for a given $\vec{V}_{ref}$; b) Perform the minimization problem, as outlined in [6], for each of these sets of vectors; c) Identify which choice results in minimum among all of the optimal lengths of the applied average voltage vector in $z_1 - z_2$ plane. *With large number of such choices, it is difficult to follow the procedure outlined above.*

To find the best technique(s), that results in global minimum length of the applied average voltage vector in $z_1 - z_2$ plane in overmodulation region, a general method is presented in section-III which doesn't require to decide the switching states beforehand.

III. Minimization of Harmonic Injection in Overmodulation

A. Expressing 6ϕ space-vectors in terms of 3ϕ space-vectors

Equation (2a) and (2b) apply the standard $3\phi - 3\phi$ Clarke's transformation C on the line-neutral voltages of two 3ϕ inverters. Here, the prime denotes the quantities related to second inverter. One should note here that $\underline{\alpha} - \underline{\beta}$ is 3ϕ transformed domain and different from 6ϕ $\alpha - \beta$. With (1), (2a) and (2b), the average voltage vectors in $\alpha - \beta$ and $z_1 - z_2$ planes can be written as the linear combination of average voltage vectors of two three-phase inverters, as shown in (3). Here, $*$ denotes conjugate operation. According to 3ϕ inverter literature, $\overline{v}_{\underline{\alpha}} + j\overline{v}_{\underline{\beta}}$ and $\overline{v}'_{\underline{\alpha}} + j\overline{v}'_{\underline{\beta}}$ are the average voltage space-vectors of the inverter-1 and inverter-2, respectively.

$$\underbrace{\begin{bmatrix} v_{\underline{\alpha}} \\ v_{\underline{\beta}} \\ v_{\underline{o}} \end{bmatrix}}_{V_{\underline{\alpha}\underline{\beta}\underline{o}}} \triangleq \underbrace{\frac{1}{\sqrt{3}} \begin{bmatrix} 1 & -\frac{1}{2} & -\frac{1}{2} \\ 0 & \frac{\sqrt{3}}{2} & -\frac{\sqrt{3}}{2} \\ 1 & 1 & 1 \end{bmatrix}}_{C} \underbrace{\begin{bmatrix} v_{ao} \\ v_{bo} \\ v_{co} \end{bmatrix}}_{V_{abc}} \tag{2a}$$

$$\begin{bmatrix} v'_{\underline{\alpha}} & v'_{\underline{\beta}} & v'_{\underline{o}} \end{bmatrix}^T \triangleq C \begin{bmatrix} v_{a'o'} & v_{b'o'} & v_{c'o'} \end{bmatrix}^T \tag{2b}$$

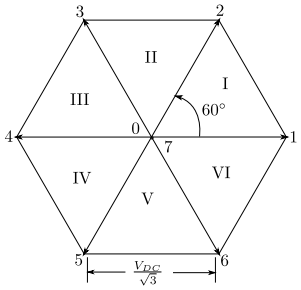

Fig. 3: Voltage vectors of three-phase inverter

$$\vec{V}_{ref} \triangleq \overline{v}_{\alpha} + j\overline{v}_{\beta} = \underbrace{\left(\overline{v}_{\underline{\alpha}} + j\overline{v}_{\underline{\beta}}\right)}_{x_1+jy_1} + \underbrace{\left(\overline{v}'_{\underline{\alpha}} + j\overline{v}'_{\underline{\beta}}\right) e^{j30^\circ}}_{x_2+jy_2} \tag{3a}$$
$$= (x_1 + x_2) + j(y_1 + y_2)$$

$$\overline{v}_{z_1} + j\overline{v}_{z_2} = \left(\underbrace{\left(\overline{v}_{\underline{\alpha}} + j\overline{v}_{\underline{\beta}}\right)}_{x_1+jy_1} - \underbrace{\left(\overline{v}'_{\underline{\alpha}} + j\overline{v}'_{\underline{\beta}}\right) e^{j30^\circ}}_{x_2+jy_2} \right)^* \tag{3b}$$
$$= (x_1 - x_2) - j(y_1 - y_2)$$

B. Objective function, equality and inequality constraints

To minimize the applied RMS voltage in $z_1 - z_2$ plane, applied average voltage vector length over each switching cycle needs to be minimized. Therefore, (4) is the objective function which can be derived from (3b). As we want to minimize this objective function for the given $\overline{v}_{\alpha}$ and $\overline{v}_{\beta}$, the real and imaginary parts of (3a), i.e., $x_1 + x_2 = \overline{v}_{\alpha}$ and $y_1 + y_2 = \overline{v}_{\beta}$, are two equality constraints in this problem.

$$|\overline{v}_{z_1} + j\overline{v}_{z_2}|^2 = (x_1 - x_2)^2 + (y_1 - y_2)^2 \tag{4}$$

Fig. 3 shows the mapping of line-neutral voltages generated by 8 switching states (2 zero states and 6 active states) of two-level 3ϕ inverter into $\underline{\alpha} - \underline{\beta}$ in accordance with (2a). Due to balanced load with isolated neutral configuration, voltage generated by these states in $\underline{o}$ plane is zero. By joining the tips of 6 active vectors, a regular hexagon is obtained with length of each side equal to $\frac{V_{DC}}{\sqrt{3}}$. The duty ratios of the six switches of 3ϕ inverter should be between 0 to 1 and summation of all the duty ratios, corresponding to the switching states applied within a switching cycle, should be equal to 1. With these duty-ratio constraints, the average voltage space-vectors generated by individual 3ϕ inverter, $\overline{v}_{\underline{\alpha}} + j\overline{v}_{\underline{\beta}}$ and $\overline{v}'_{\underline{\alpha}} + j\overline{v}'_{\underline{\beta}}$, will lie within this regular hexagon. As $x_1 + jy_1 \triangleq \overline{v}_{\underline{\alpha}} + j\overline{v}_{\underline{\beta}}$, $x_1 + jy_1 \in B_1$, where B_1 is same as hexagon of Fig. 3. As $x_2 + jy_2 \triangleq (\overline{v}'_{\underline{\alpha}} + j\overline{v}'_{\underline{\beta}})e^{j30^\circ}$, $x_2 + jy_2 \in B_2$, where B_2 is obtained by rotating the hexagon of Fig. 3 by 30° in anti-clockwise direction. In Fig. 4, B_1 and B_2 are shown in black and red colours; lengths are normalized with respect to V_{DC}. These boundaries of $x_1 + jy_1$ and $x_2 + jy_2$ are the inequality constraints in this problem which are arising due to duty-ratio constraints of the switches of 6ϕ inverter.

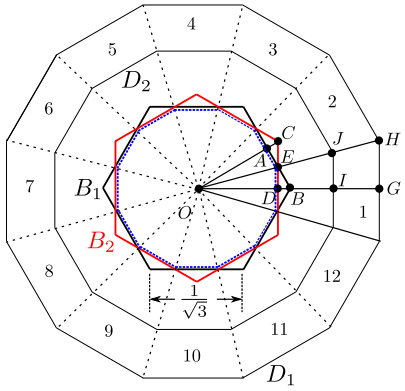

Fig. 4: B_1, B_2, D_1 and D_2

C. Identification of overmodulation region

With the constraints $(x_1+jy_1) \in B_1$ and $(x_2+jy_2) \in B_2$, (3a) gives us all possible $\overline{v}_\alpha+j\overline{v}_\beta$ which lie within do-decagon D_1 of Fig. 4. D_1 is same as the do-decagon in $\alpha-\beta$ plane of Fig. 2. In linear modulation range, $\overline{v}_{z_1} = \overline{v}_{z_2} = 0$. According to (3b), the only way to achieve this is by applying $x_1 = x_2$ and $y_1 = y_2$, which implies $x_1 + jy_1 = x_2 + jy_2$. With this constraint, the maximum boundary of $x_1 + jy_1$ (or $x_2 + jy_2$) takes the shape of a do-decagon which is shown by the dotted blue line in Fig. 4. Summation of the voltage vectors, x_1+jy_1 and x_2+jy_2, along this blue line gives the mapping of $\overline{v}_\alpha+j\overline{v}_\beta$ in linear region (according to (3a)) and is shown by the do-decagon D_2 in Fig. 4. Therefore, region between D_1 and D_2 is the region of OVM of ASPM.

Due to structural symmetry of D_1, whole $\alpha-\beta$ plane can be divided in 12 equivalent sectors, as shown in Fig. 4. Hence, modulation of 6ϕ drive will be discussed only for sector-1 and modulation of the remaining sectors will be similar to sector-1. Moreover, B_1, B_2, D_1 and D_2 are symmetric with respect to real axis. Therefore, discussion of modulation is further restricted to upper half of sector-1 and zoomed version of this part is shown separately in Fig. 5.

D. Minimization in OVM region of upper-half of sector-1

AB, CD, JI and HG in Fig. 5 are parts of B_1, B_2, D_2 and D_1, respectively. $\angle OBA = \angle OCD = 60°$, $\angle COD = 30°$ (as B_2 is rotated by 30°), $\therefore \angle ODC = 90°$. As $OB = OC = \frac{1}{\sqrt{3}}$, $OD = OC\cos 30° = \frac{1}{2}$. For $\overline{v}_\alpha + j\overline{v}_\beta \triangleq \vec{V}_{ref}$ lying within ΔOHG, we will argue that $x_1 + jy_1 \in \Delta OAB$ and $x_2 + jy_2 \in \Delta OCD$. ΔOHG consists of two regions- linear region, ΔOJI, and OVM region, $\square IJHG$. Therefore, we want to determine x_1+jy_1 and x_2+jy_2 when tip of $\vec{V}_{ref} \in \square IJHG$.

For tip of $\vec{V}_{ref} \in \square IJHG$, it is possible to show that two inequality constraints out of six (three boundaries of each of ΔOAB and ΔOCD) become active, viz., $x_1 + jy_1$ is in that side of AB where origin, O, is there and x_2+jy_2 is in the left side of CD. Equation of straight line AB, which makes an intercept of $\frac{1}{\sqrt{3}}$ along X with a slope of $\tan 120°$, is $\sqrt{3}X + Y = 1$. Equation of CD is $X = \frac{1}{2}$. Therefore, active inequality constraints are as follows.

$$\sqrt{3}x_1 + y_1 \le 1 \quad \text{(5a)} \qquad\qquad x_2 \le \frac{1}{2} \quad \text{(5b)}$$

1) Four variables to two variables problem: Substituting x_2 and y_2 from the two equality constraints in objective function, (4), and two active inequality constraints, (5a) and (5b), the minimization problem becomes as (6), where $\overline{v}_\alpha$ and $\overline{v}_\beta$ appear as parameters. This optimization problem boils down to determine a point within the feasible region, defined by the inequality constraints of (6), in $x_1 - y_1$ plane so that the distance between that point and the point with co-ordinates $(\frac{\overline{v}_\alpha}{2}, \frac{\overline{v}_\beta}{2})$ is minimized.

$$\underbrace{\min_{\substack{\sqrt{3}x_1+y_1\le 1 \\ x_1 \ge \overline{v}_\alpha - \frac{1}{2}}} \left(x_1 - \frac{\overline{v}_\alpha}{2}\right)^2 + \left(y_1 - \frac{\overline{v}_\beta}{2}\right)^2}_{(\overline{v}_\alpha + j\overline{v}_\beta) \in \square IJHG} \quad (6)$$

2) Inequality constraints and search space for optimal solution in x_1-y_1 plane: Fig. 6 helps to visualize this problem geometrically in $x_1 - y_1$ plane. The boundary of the first inequality constraint of (6), i.e., $\sqrt{3}x_1 + y_1 \le 1$, is shown by AB. The boundary of the second inequality constraint, i.e., $x_1 \ge \overline{v}_\alpha - \frac{1}{2}$, is shown by RS. The x_1-intercept of RS varies as $\overline{v}_\alpha$ changes. The regions in x_1-y_1 plane, which satisfy the above two inequality constraints, are shown by double-lined arrows on AB and RS. AB and RS intersect each other at E'. Therefore, $\Delta E'SB$ (shaded region) in Fig. 6, intersection of the above two regions, is the feasible search space for optimal solution.

3) Modified minimization problem in $x_1 - y_1$ plane: As discussed earlier, solving the minimization problem of (6) is equivalent to determine a point within $\Delta E'SB$ so that distance between that point and the point with co-ordinates $(\frac{\overline{v}_\alpha}{2}, \frac{\overline{v}_\beta}{2})$, suppose P, is minimized. As the co-ordinates of both $E'S$ boundary of feasible search space and the point P are functions of $\overline{v}_\alpha$ and $\overline{v}_\beta$, we will try to trace $E'S$ and P for all possible $(\overline{v}_\alpha + j\overline{v}_\beta) \in \square IJHG$. The OVM region, $\square IJHG$, can be identified by checking (7).

$$C_1 : \overline{v}_\alpha - 1 > 0 \quad (7)$$

Any point within $\square IJHG$ of Fig. 5 has $\overline{v}_\alpha$ and $\overline{v}_\beta$ in the following range- $1 \le \overline{v}_\alpha \le \frac{1}{2} + \frac{1}{\sqrt{3}}$ and $0 \le \overline{v}_\beta \le \overline{v}_\alpha \tan 15°$, for the corresponding $\overline{v}_\alpha$. Therefore, $\frac{1}{2} = OD \le \overline{v}_\alpha - \frac{1}{2} = OS \le \frac{1}{\sqrt{3}} = OB$ is true for all possible $(\overline{v}_\alpha, \overline{v}_\beta)$ within $\square IJHG$. Let us consider a line KL parallel to Y-axis within $\square IJHG$ such that KL intersects OH and OG at K and L, respectively, in Fig. 5. By varying KL from JI to HG, we can trace each point within $\square IJHG$. Suppose, we want to solve the optimization problem for a point $(\overline{v}_\alpha, \overline{v}_\beta)$ lying on the line KL. Corresponding $(\frac{\overline{v}_\alpha}{2}, \frac{\overline{v}_\beta}{2})$ will be on $K'L'$ line in Fig. 6, where $OL' = \frac{\overline{v}_\alpha}{2}$. As $K'L' = OL' \tan 15°$, K' will be on the line OE. As $\overline{v}_\alpha \ge 1$ for any point within $\square IJHG$, $\frac{1}{2} = OD \le \frac{\overline{v}_\alpha}{2} = OL' \le \overline{v}_\alpha - \frac{1}{2} = OS$. Therefore, $K'L'$ will always be in the left-hand side of RS and right-hand side of ED for $(\overline{v}_\alpha + j\overline{v}_\beta) \in \square IJHG$.

Let, the line drawn from point E' parallel to x_1 axis intersects $K'L'$ at E''. The y_1 coordinate of E' or E'' can be determined by solving the equations of the lines AB and RS, which gives $E'S = E''L' = (1+\frac{\sqrt{3}}{2}) - \sqrt{3}\overline{v}_\alpha$. Depending

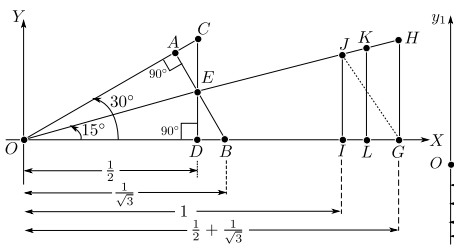

Fig. 5: Zoomed upper half of sector-1

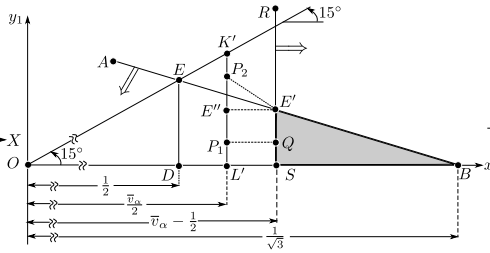

Fig. 6: Problem in $x_1 - y_1$ plane

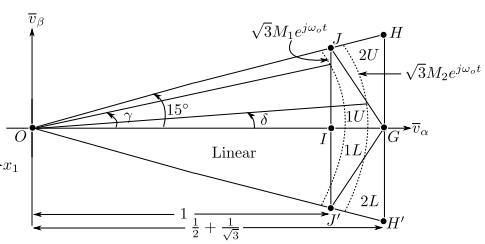

Fig. 7: Four sub-sectors in sector-1

upon the position of the point with co-ordinates $(\frac{\overline{v}_\alpha}{2}, \frac{\overline{v}_\beta}{2})$ on $K'L'$, two cases may arise.

OVM-Case-1: The point lie on $E''L' \implies \frac{\overline{v}_\beta}{2} \leq E''L'$

P_1 is such a point in Fig. 6. As shown in Fig. 6, Q is the point which is at minimum distance from P_1 within feasible region $E'SB$. Therefore, optimal solution, $x^*_{1,2}$ and $y^*_{1,2}$, are given in (8). With these solutions, optimum $z_1 - z_2$ plane voltages can be determined from (3b) and are given in (8). The condition $\frac{\overline{v}_\beta}{2} \leq E''L'$ is equivalent to (9). Equation of the line passing through G and J in Fig. 5 is $\sqrt{3}X + \frac{Y}{2} = (1 + \frac{\sqrt{3}}{2})$ (shown by dotted line). Therefore, this case arises when tip of $\vec{V}_{ref}$ lies within ΔIGJ of Fig. 5.

$$\begin{aligned} &x^*_1 = \overline{v}_\alpha - \frac{1}{2}; \quad y^*_1 = \frac{\overline{v}_\beta}{2}; \quad x^*_2 = \frac{1}{2}; \quad y^*_2 = \frac{\overline{v}_\beta}{2} \\ &\overline{v}^*_{z_1} = \overline{v}_\alpha - 1; \quad \overline{v}^*_{z_2} = 0 \end{aligned} \tag{8}$$

$$C_2 : \frac{\overline{v}_\beta}{2} \leq (1 + \frac{\sqrt{3}}{2}) - \sqrt{3}\overline{v}_\alpha \implies \sqrt{3}\overline{v}_\alpha + \frac{\overline{v}_\beta}{2} \leq (1 + \frac{\sqrt{3}}{2}) \tag{9}$$

$$\begin{aligned} &x^*_1 = \overline{v}_\alpha - \frac{1}{2}; \quad y^*_1 = (1 + \frac{\sqrt{3}}{2}) - \sqrt{3}\overline{v}_\alpha \\ &x^*_2 = \frac{1}{2}; \quad y^*_2 = \sqrt{3}\overline{v}_\alpha + \overline{v}_\beta - (1 + \frac{\sqrt{3}}{2}) \\ &\overline{v}^*_{z_1} = \overline{v}_\alpha - 1; \quad \overline{v}^*_{z_2} = 2\sqrt{3}\overline{v}_\alpha + \overline{v}_\beta - (2 + \sqrt{3}) \end{aligned} \tag{10}$$

OVM-Case-2: The point lie on $K'E'' \implies \sqrt{3}\overline{v}_\alpha + \frac{\overline{v}_\beta}{2} > (1 + \frac{\sqrt{3}}{2}) \implies$ tip of $\vec{V}_{ref} \in \Delta GHJ$ of Fig. 5.

P_2 is such a point in Fig. 6. In this case, E' is the closest point from $(\frac{\overline{v}_\alpha}{2}, \frac{\overline{v}_\beta}{2})$ within the feasible region. The optimal solution in this case is given in (10).

E. Minimization in OVM region of lower-half of sector-1

Similar to upper-half of sector-1, the optimal solution for OVM region of lower half of sector-1 can be determined. Fig. 7 shows the four overmodulation regions in sector-1 where **OVM-Case-1** and **OVM-Case-2** in upper-half and lower-half are denoted by $1U$, $2U$ and $1L$, $2L$, respectively. The inequality through which $2L$ is differentiated from $1L$ is given in (11). The optimal solution in $1L$ is same as (10) whereas optimal solution in $2L$ is given by (12).

$$C_3 : \sqrt{3}\overline{v}_\alpha - \frac{\overline{v}_\beta}{2} > (1 + \frac{\sqrt{3}}{2}) \tag{11}$$

$$\begin{aligned} &x^*_1 = \overline{v}_\alpha - \frac{1}{2}; \quad y^*_1 = \sqrt{3}\overline{v}_\alpha - (1 + \frac{\sqrt{3}}{2}) \\ &x^*_2 = \frac{1}{2}; \quad y^*_2 = -\sqrt{3}\overline{v}_\alpha + \overline{v}_\beta + (1 + \frac{\sqrt{3}}{2}) \\ &\overline{v}^*_{z_1} = \overline{v}_\alpha - 1; \quad \overline{v}^*_{z_2} = -2\sqrt{3}\overline{v}_\alpha + \overline{v}_\beta + (2 + \sqrt{3}) \end{aligned} \tag{12}$$

As discussed before, the optimal solution in linear region, i.e., when $\overline{v}_\alpha \leq 1$ or tip of $\vec{V}_{ref} \in \Delta OIJ$ of Fig. 5, can be determined by plugging $\overline{v}_{z_1} = \overline{v}_{z_2} = 0$ in (3) and given below.

$$x^*_1 = x^*_2 = \frac{\overline{v}_\alpha}{2}; \quad y^*_1 = y^*_2 = \frac{\overline{v}_\beta}{2} \tag{13}$$

It should be noted here that optimum $\overline{v}_{z_1}$ and $\overline{v}_{z_2}$, as given in (8), (10) and (12), are similar to the optimum solution obtained by *SVOVM4-2* in [6] (refer equations (27), (34) and (36) of [6]). The constant terms differ due to different scaling factor in the transformation matrix T. Therefore, *SVOVM4-2* is one of the ways to achieve the global minima of harmonic voltage injection. There are few more ways to attain the optimal technique, which are discussed in the next section.

IV. Optimal SVOVM Techniques

The optimal SVOVM techniques of the aforementioned two OVM cases in upper-half of sector-1 are derived in this section based on the analysis of the previous section. During selection of switching sequences, *simultaneous switching of two legs of the 6ϕ inverter* and *active-vector splitting* are not accounted.

A. Switching Sequences for **OVM-Case-1**

1) Individual inverter state identification: (8) gives the optimal solution for this case. As $x^*_2 = \frac{1}{2}$, $(\overline{v}'_{\underline{\alpha}} + j\overline{v}'_{\underline{\beta}})e^{j30^\circ} = x_2 + jy_2$ lies on line DC of Fig. 5 or $\overline{v}'_{\underline{\alpha}} + j\overline{v}'_{\underline{\beta}}$ lies on the side of the hexagon of Fig. 3 which is obtained by joining states 1 and 6. Therefore, inverter-2 has to apply states $1'$ and $6'$ and summation of the duty ratios, for which these states are applied, is 1, i.e., $d_{1'} + d_{6'} = 1$. In (8), $\sqrt{3}x_1 + y_1 < 1$. As $\overline{v}_{\underline{\alpha}} = x_1$ and $\overline{v}_{\underline{\beta}} = y_1$, according to (3a), $\sqrt{3}\overline{v}_{\underline{\alpha}} + \overline{v}_{\underline{\beta}} < 1$. This implies $\overline{v}_{\underline{\alpha}} + j\overline{v}_{\underline{\beta}} \in \Delta OAB$ in Fig. 5. We know that any vector within 30° of sector-I of hexagon of Fig. 3 can be realized by using either $\{6, 1, 2\}$ states or $\{z, 1, 2\}$ states; where z is zero state and $z \in \{0, 7\}$. Therefore, both $\{6, 1, 2\}$ or $\{z, 1, 2\}$ are possible states of inverter-1 to realize (8).

2) 6ϕ inverter state identification and sequence design: It can be shown that $d_1 \geq d_{1'} \geq d_{6'} \geq (d_2 + d_{6/z})$ is true in this case. Fig. 8a and 8b show the possible states and sequences to achieve the optimal solution when inverter-1 applies $\{6, 1, 2\}$ and $\{z, 1, 2\}$, respectively. Position of $1'$ and $6'$ have been kept fixed and relative positions of states of inverter-1 are changed in this figure. Fig. 8b is further split into 3 cases depending on applied zero state: 0, 7 and both 0 and 7 are applied in cases b1, b2 and b3. Table II tabulates the states and sequences generated by different cases of Fig. 8. The switching signal waveforms are symmetric over the sampling period, T_s. It can be seen from table II that both four and five active vectors

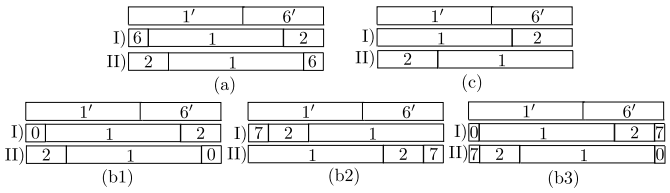

Fig. 8: Possible switching states of six-phase inverter in overmodulation. (a) **OVM-Case-1** ($1U$) and inverter-1 applies $\{6, 1, 2\}$. (b) **OVM-Case-1** ($1U$) and inverter-1 applies $\{z, 1, 2\}$. (c) **OVM-Case-2** ($2U$).

can be used to attain optimal solution. Therefore, 8 possible sequences are derived in this case.

B. Switching Sequences for OVM-Case-2

1) Individual inverter state identification: The optimal solution in (10) satisfies $\sqrt{3}x_1 + y_1 = 1$ and $x_2 = \frac{1}{2}$. Therefore, $\overline{v}_{\underline{\alpha}} + j\overline{v}_{\beta}$ lies on line AB of Fig. 5. As AB is part of the side of the hexagon of Fig. 3, obtained by joining states 1 and 2, therefore (10) can only be realized with states 1 and 2 of inverter-1 with $d_1 + d_2 = 1$ Inverter-2 will apply states 6 and 1, as before.

2) 6ϕ inverter state identification and sequence design: It is possible to show that $d_1 \geq d_{1'} \geq d_{6'} \geq d_2$ holds in this case. Fig. 8c shows possible 2 sequences where only 3 vectors can be used. Table II lists these sequences.

C. Derivation of optimal Techniques

Combining the above 8 possible sequences for **OVM-Case-1** and 2 sequences for **OVM-Case-2**, one can have 16 optimal PWM techniques in the whole OVM region.

Existing *SVOVM4-2* uses case a-I in ΔIGJ and case c-I in ΔGJH. A carrier comparison based implementation of this optimal technique is discussed in the next section which results into sequence b3-I in ΔIGJ (2 large, 1 medium and 2 small (2L+1M+2S) active vectors in $\alpha - \beta$) and c-I (2 large, 1 medium (2L+1M) vectors) in ΔGJH. Although all of the techniques of table II inject optimal low-frequency voltages in $z_1 - z_2$ plane, their high-frequency performances, like, current ripple, flux ripple are expected to differ similar to linear techniques of ASPM. Similar to sector-1, the optimal solutions and sequence of active vectors for other sectors of do-decagon D_1 of Fig. 4 can be derived.

D. Average switching frequency in OVM region

Let, the average commutation over one $T_s = \frac{1}{F_s}$ is defined as the ratio of number of legs switch over one T_s and total number of legs (it is 6 for 6ϕ inverter). Table II lists the average commutation of different techniques in OVM. For $0.577 < M \leq 0.5977$, circular $\vec{V}_{ref} = \sqrt{3}Me^{j\omega_o t}$ lies in $1U$ for $0° \leq \omega_o t \leq \gamma(M) = \cos^{-1}\frac{1}{\sqrt{3}M}$ and in linear region for $\gamma(M) < \omega_o t \leq 15°$ in upper-half of sector-1 and $\vec{V}_{ref}$ never enters in $2U$, as shown in Fig. 7 with $M = M_1$. For $0.5977 < M \leq 0.622$, circular $\vec{V}_{ref}$ lies in $1U$ for $0° \leq \omega_o t \leq \delta(M) = \sin^{-1}(\frac{2+\sqrt{3}}{\sqrt{39}M}) - \tan^{-1}(2\sqrt{3})$ and in $2U$ for $\delta(M) < \omega_o t \leq 15°$ in upper-half of sector-1 and it never enters in linear region in this modulation index range, as shown in Fig. 7 with $M = M_2$. If conventional SVPWM technique is adopted per 3ϕ inverters in linear region where

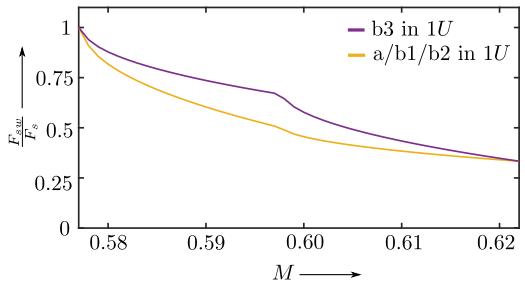

Fig. 9: $\frac{F_{sw}}{F_s}$ as function of M

all legs switches, average commutation in linear region is 1. Therefore, average switching frequency, F_{sw}, of 6ϕ inverter over $15°$ for $0.577 < M \leq 0.5977$ is given by (14) and for $0.5977 < M \leq 0.622$ is given by (15). As modulation over $360°$ is symmetrical for all 6 legs, the average switching frequency over fundamental period is same as (14) and (15). Fig. 9 plots $\frac{F_{sw}}{F_s}$ as function of M for $0.577 \leq M \leq 0.622$. Based on the technique used when tip of $\vec{V}_{ref}$ lie in $1U$, either a/b1/b2 or b3 (average commutation is $\frac{1}{2}$ or $\frac{2}{3}$), two plots are given.

$$F_{sw} = F_s \frac{(15° - \gamma(M)) \times 1 + \gamma(M)) \times (\frac{1}{2} \text{ or } \frac{2}{3})}{15°} \quad (14)$$

$$F_{sw} = F_s \frac{(15° - \delta(M)) \times \frac{1}{3} + \delta(M) \times (\frac{1}{2} \text{ or } \frac{2}{3})}{15°} \quad (15)$$

V. Carrier-comparison based Implementation of Optimal Technique

Following steps are followed in order to determine the six duty-ratios of top six switches of 6ϕ inverter from the given $\overline{v}_{\alpha}, \overline{v}_{\beta}$.

Step-1 Sector Identification: Find k, so that $30°k - 45° \leq \angle(\overline{v}_{\alpha} + j\overline{v}_{\beta}) \leq 30°k - 15°$

Step-2 Determination of voltages in modulo-sector: Find $\overline{v}_{\alpha m} + j\overline{v}_{\beta m} = (\overline{v}_{\alpha} + j\overline{v}_{\beta})e^{-j(k-1)30°}$.

Step-3 Sub-sector Identification: Use conditions C_1, C_2, and C_3 of section-III to determine if the modulo vector lies in linear, $2U$, $2L$ or $1U/1L$.

Step-4 Determination of optimal solution: Using (13) (linear), (8) ($1U$ and $1L$), (10) ($2U$) and (12) ($2L$), find optimal x_1, y_1, x_2 and y_2. If k is odd, $x_{1m} + jy_{1m} = x_1 + jy_1$; $x_{2m} + jy_{2m} = x_2 + jy_2$. If k is even, $x_{1m} + jy_{1m} = x_2 + jy_2$; $x_{2m} + jy_{2m} = x_1 + jy_1$.

Step-5 Determination of optimal space-vectors: The space-vectors corresponding to k^{th} sector can be found as, $(\overline{v}_{\underline{\alpha}} + j\overline{v}_{\beta}) \triangleq (x_1 + jy_1) = (x_{1m} + jy_{1m})e^{j(k-1)30°}$; $(\overline{v}'_{\underline{\alpha}} + j\overline{v}'_{\beta}) = (x_{2m} + jy_{2m})e^{j(k-2)30°}$.

Step-6 Calculation of modulation signals: Using inverse Clarke's transformation of (2), $\overline{v}_{ao}$, $\overline{v}_{bo}$,...$\overline{v}_{c'o'}$ can be determined.

Step-7 Calculation of Six duty ratios: Duty ratios of the top switches of six legs, d_a, d_b...$d_{c'}$, can be calculated by adopting conventional SVPWM technique per 3ϕ inverters where $\frac{1}{2} + \frac{mid}{2}$ common-mode signals to individual 3ϕ inverters are injected. This results into application of two zero states (0 and 7 in Table I) for equal duration of time.

14 comparisons, 18 additions and 17 multiplications are required to follow the above steps. As Inverter-1 applies both

TABLE II: Optimal Sequences in OVM (Tip of $\vec{V}_{ref} \in \square IJHG$)

OVM Zone	Case	Switching sequence over T_s	Vector type	Avg. commutation over T_s
$1U$	a-I	$(6,1') - (1,1') - (1,6') - (2,6') - (1,6') - (1,1') - (6,1')$	2L+2M	$\frac{1}{2}$
	a-II	$(2,1') - (1,1') - (1,6') - (6,6') - (1,6') - (1,1') - (2,1')$	4L	
	b1-I	$(0,1') - (1,1') - (1,6') - (2,6') - (1,6') - (1,1') - (0,1')$	2L+1M+1S	
	b1-II	$(2,1') - (1,1') - (1,6') - (0,6') - (1,6') - (1,1') - (2,1')$	3L+1S	
	b2-I	$(7,1') - (2,1') - (1,1') - (1,6') - (1,1') - (2,1') - (7,1')$	3L+1S	
	b2-II	$(1,1') - (1,6') - (2,6') - (7,6') - (2,6') - (1,6') - (1,1')$	2L+1M+1S	
	b3-I	$(0,1') - (1,1') - (1,6') - (2,6') - (7,6') - (2,6') - (1,6') - (1,1') - (0,1')$	2L+1M+2S	$\frac{2}{3}$
	b3-II	$(7,1') - (2,1') - (1,1') - (1,6') - (0,6') - (1,6') - (1,1') - (2,1') - (7,1')$	3L+2S	
$2U$	c-I	$(1,1') - (1,6') - (2,6') - (1,6') - (1,1')$	2L+1M	$\frac{1}{3}$
	c-II	$(2,1') - (1,1') - (1,6') - (1,1') - (2,1')$	3L	

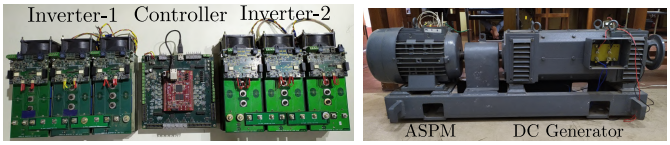

(a) (b)

Fig. 10: Experimental set-up. (a) Six-phase inverter and controller. (b) ASPM coupled with DC generator.

TABLE III: Steady-state Circuit Parameters of 6ϕ IM

Per phase stator and rotor resistances (r_s, r_r)	0.675 Ω
Per phase stator and rotor leakage inductances (L_{ls}, L_{lr})	3.75 mH
Per phase self-inductance of stator and rotor (L_s, L_r)	0.172 H
Per phase mutual inductance ($L_M = L_s - L_{ls}$)	0.168 H

zero states (0 and 7) equally and Inverter-2 doesn't apply any zero state as the dwell time of zero-state is zero, it results into b3-I in $1U$. In $2U$, dwell times of zero-states of both of the inverters are zero. But, as all the duty signals are compared with same triangular carrier, it results into c-I.

VI. Experimental and Simulation Results

To validate the proposed optimal technique experimentally, asymmetrical squirrel-cage 6ϕ induction motor (IM) is chosen as the 6ϕ machine. The specification of ASPM is 5 kW, 2 pole, 120 V line-neutral RMS in 6ϕ configuration, 50 Hz. This machine is coupled with 5 kW DC generator which acts as load. The six phases are fed from two 3ϕ inverters which are built with 1200 V, 75 A SEMIKRON IGBT (SKM75GB123D) module. The controller card consists of Zynq-7010 IC, which has both processing system and programmable hardware, and customized interface card to generate PWM signals for the switches. The experimental set-up is shown in Fig. 10. Table III tabulates the steady-state equivalent circuit parameters of 6ϕ-IM, where winding resistance and leakage inductance of per-phase stator equivalent circuit in $\alpha-\beta$ and z_1-z_2 are r_s and L_{ls}, respectively; mutual inductance, L_M, only appears in $\alpha-\beta$. Using these parameters, dynamic model of the machine is implemented in Matlab Simulink to verify the proposed technique through simulation.

TABLE IV: Operating Conditions of Experiments and Simulations

Peak fundamental line-neutral voltage (V_o)	$120\sqrt{2}$ V
Fundamental frequency (f_o)	50 Hz
Output power	3.5 kW
Switching frequency	5 kHz

Experiments and simulations are performed at eleven values of M within $0.577 \leq M \leq 0.622$. Table IV shows the operating condition for each of these experiments. As $V_o = MV_{DC} = 120\sqrt{2}$ V, V_{DC} is changed with M in order to keep V_o and f_o constant for all M, although it is customary to keep V_{DC} constant and change f_o with M accordingly. Fig. 11 shows experimental and simulated waveforms of proposed technique. Fig. 11a and 11d show the experimental and simulated waveforms of i_a and $i_{a'}$, respectively, at $M = 0.612$ which are at a phase difference of 30°. Similarly, 30° phase-shifted line-line voltage waveforms, v_{ab} and $v_{a'b'}$, are shown in Fig. 11c and 11f. 3ϕ currents of one of the inverters are shown in Fig. 11b and 11e. They are at 120° phase difference to each other. The 3ϕ currents of the other inverter are also similar and they are at 30° phase difference to these set of 3ϕ currents. The experimental line currents and line-line voltages at the maximum boundaries of linear and OVM region, i.e., at $M = 0.577$ and $M = 0.622$ are shown in Fig. 11g, 11j and 11h, 11k, respectively. The line currents are sinusoidal in Fig. 11g. Fig. 11i shows experimental i_α and i_β at $M = 0.622$ which are sinusoidal, although low-frequency harmonics are present in line-currents. From line-line voltage waveforms at three modulation indices, it is clear that switching frequency decreases as M increases. The harmonic spectrum of experimental and simulated line-line voltages and phase currents at $M = 0.612$ are shown in Fig. 11m, 11n, 11o and 11p. The optimal technique injects $12k \pm 5$ harmonics in $z_1 - z_2$ plane and 5^{th} and 7^{th} harmonics among them are prominent. The peak of fundamental, 5^{th} and 7^{th} harmonic components of line-line voltages, as obtained from experiment and simulation, are 285.3 V, 24.1 V, 6.5 V and 281.1 V, 23 V, 4.2 V, respectively, at $M = 0.612$. The peak of fundamental, 5^{th} and 7^{th} harmonic components of experimental and simulated phase currents are 7.9 A, 2.2 A, 0.1 A and 8.1 A, 2.2 A, 0.3 A, respectively. Simulated polar-plot of $\overline{v}^*_{z_1} + j\overline{v}^*_{z_2}$ of proposed technique, normalized with V_{DC}, is plotted in Fig. 11l for $M = 0.612$ and $M = 0.622$. At $M = 0.577$, this is zero. Fig. 11q shows the pole voltages, v_{xN}, for OVM region $1U$. Here, $x = a, b, c, a', b', c'$ and N is negative DC-bus, as shown in Fig. 1. Fig. 11q indicates the switching sequence used by *TINVOVM* technique which matches with b3-I of table II.

Fig. 12a and 12d compare analytical and simulated THD and WTHD of proposed technique with all other existing OVM techniques in the range of $0.577 \leq M \leq 0.622$. THD and WTHD of proposed technique is compared with *CSVPWM* experimentally in Fig. 12b and 12e. The continuous lines in

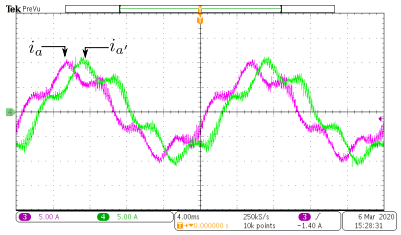

Current scale : 5 A/div. Time scale : 4 ms/div.

(a) Experimental i_a and $i_{a'}$ at $M = 0.612$

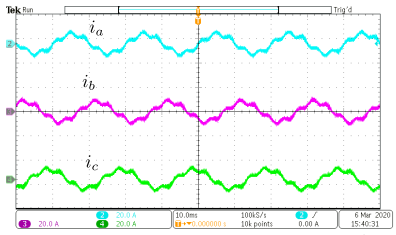

Current scale :20 A/div. Time scale : 10 ms/div.

(b) Experimental i_a, i_b, i_c at $M = 0.612$

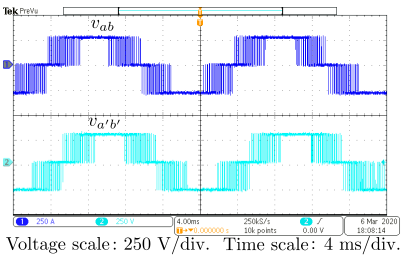

Voltage scale : 250 V/div. Time scale : 4 ms/div.

(c) Experimental v_{ab} and $v_{a'b'}$ at $M = 0.612$

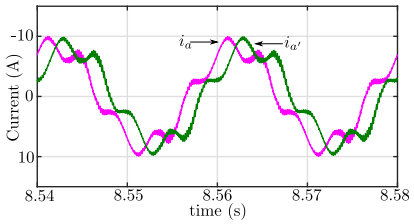

(d) Simulated i_a and $i_{a'}$ at $M = 0.612$

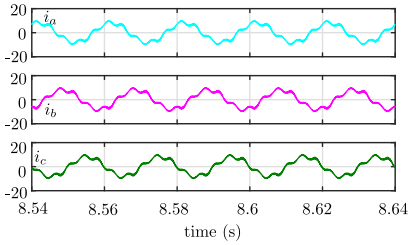

(e) Simulated i_a, i_b, i_c at $M = 0.612$

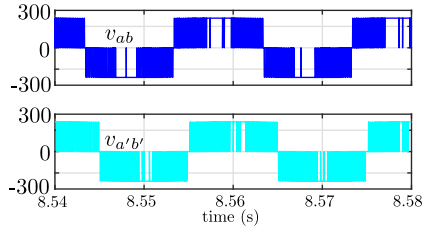

(f) Simulated v_{ab} and $v_{a'b'}$ at $M = 0.612$

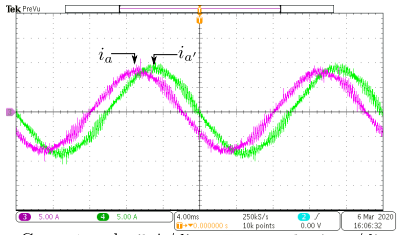

Current scale : 5 A/div. Time scale : 4 ms/div.

(g) Experimental i_a and $i_{a'}$ at $M = 0.577$

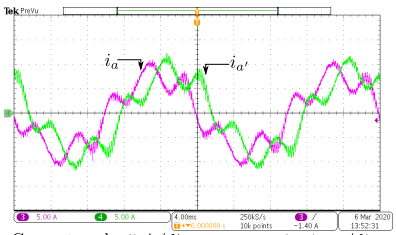

Current scale : 5 A/div. Time scale : 4 ms/div.

(h) Experimental i_a and $i_{a'}$ at $M = 0.622$

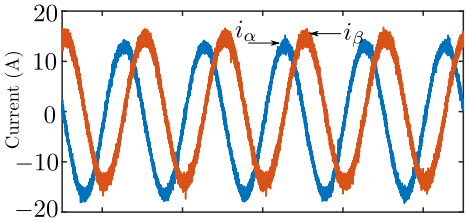

(i) Experimental i_α and i_β at $M = 0.622$

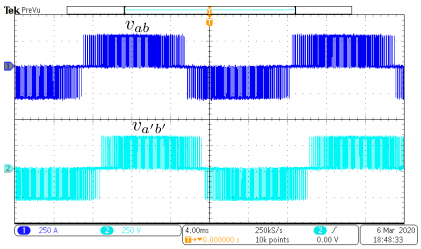

Voltage scale : 250 V/div. Time scale : 4 ms/div.

(j) Experimental v_{ab} and $v_{a'b'}$ at $M = 0.577$

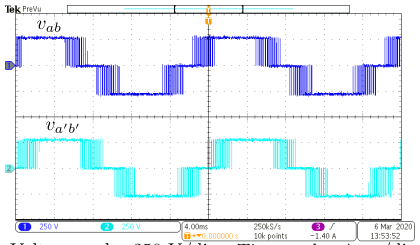

Voltage scale : 250 V/div. Time scale : 4 ms/div.

(k) Experimental v_{ab} and $v_{a'b'}$ at $M = 0.622$

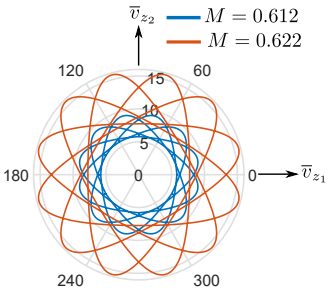

(l) polar plot of $\overline{v}^*_{z_1} + j\overline{v}^*_{z_2}$

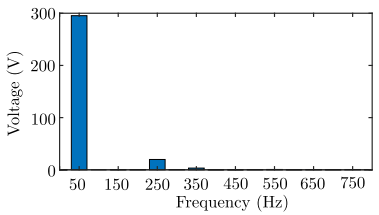

(m) Experimental v_{ab} at $M = 0.612$

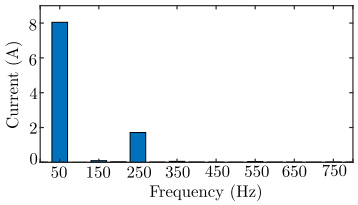

(n) Experimental i_a at $M = 0.612$

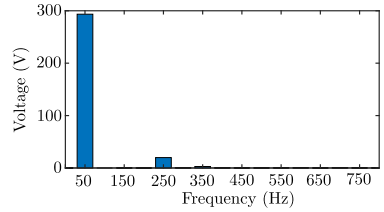

(o) Simulated v_{ab} at $M = 0.612$

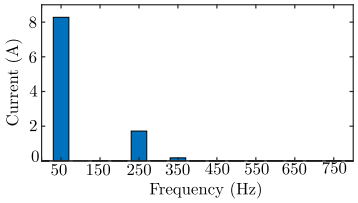

(p) Simulated i_a at $M = 0.612$

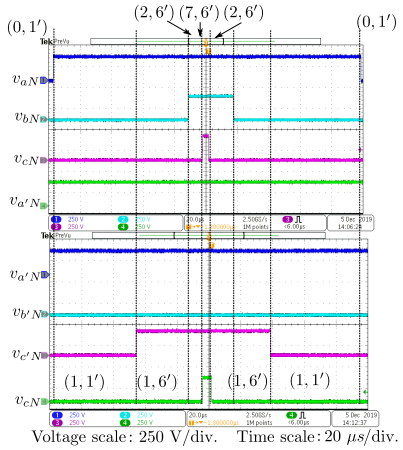

Voltage scale : 250 V/div. Time scale : 20 μs/div.

(q) Sequence of *TINVOVM* in OVM-Case-1

Fig. 11: Experimental and simulated waveforms of proposed technique

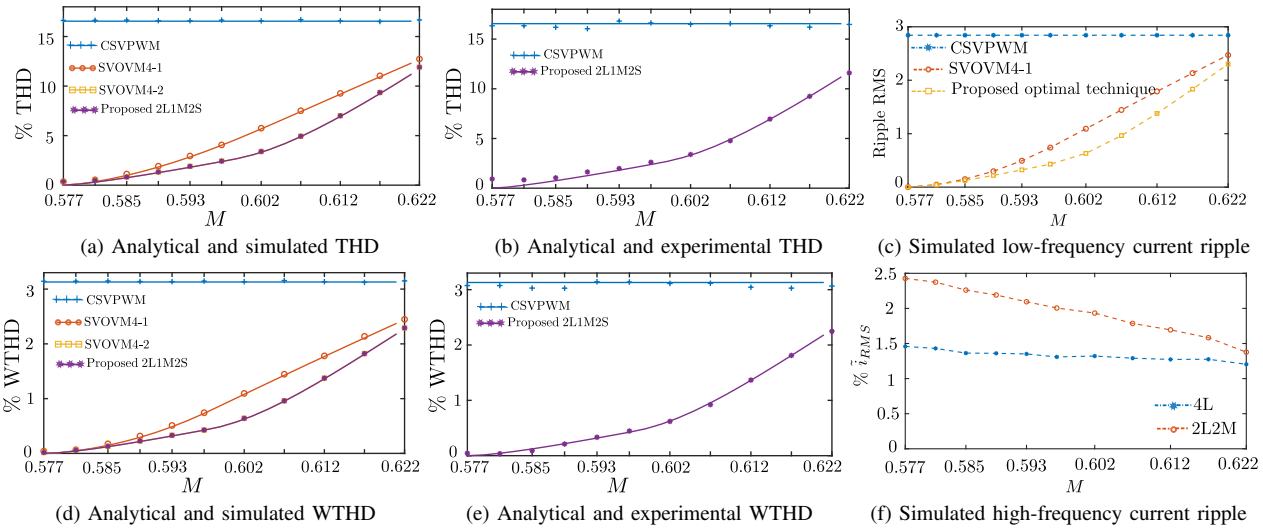

(a) Analytical and simulated THD (b) Analytical and experimental THD (c) Simulated low-frequency current ripple

(d) Analytical and simulated WTHD (e) Analytical and experimental WTHD (f) Simulated high-frequency current ripple

Fig. 12: Comparison of implemented optimal strategy (2L1M2S) with existing overmodulation techniques

these plots correspond to analytical values. The expression of WTHD is given by $WTHD = \frac{\sqrt{\sum_{n=12m\pm5}(\frac{\overline{v}_{ao}|_n}{n})^2}}{V_o}$, which is the indicator of the copper loss incurring in $z_1 - z_2$ plane. THD and WTHD performance of proposed 2L1M2S technique is similar to existing *SVOVM4-2*, as expected from analysis, and better than existing *CSVPWM* and *SVOVM4-1*. The close agreement between simulated and experimental results with analysis validates the proposed strategy. Due to dead-time of inverter or slight asymmetry in the winding, experimental THD value at $M = 0.577$ is small but non-zero, [21]. Fig. 12c compares simulated low-frequency (harmonic order less than 50) ripple RMS currents of proposed optimal techniques with other existing OVM techniques. As *SVOVM4-2* is one of the proposed techniques, it is not shown separately. Fig. 12f compares simulated RMS high-frequency (harmonic order more than 50) ripple currents of 2L2M based *SVOVM4-2* and one 4L based optimal technique which uses a-II in $1U$ and c-II in $2U$ in OVM. The performance of later is better and this justifies our claim that high-frequency ripple current performances of different optimal techniques are different.

VII. Conclusions and Future Work

This paper expresses the average voltage space-vectors of 6ϕ inverter in $\alpha - \beta$ and $z_1 - z_2$ subspaces as a linear combination of average voltage vectors of two 3ϕ inverters. Using these expressions, the paper formulates the problem of minimization of length of the applied average voltage vector of $z_1 - z_2$ subspace in each switching cycle in terms of 3ϕ space-vectors. Here, active vectors need not to be specified a priori and hence the formulation is different from the minimization strategy of existing SVOVM techniques of 6ϕ inverter. The proposed formulation achieves the optimal RMS voltage injection throughout the whole overmodulation (OVM) region, i.e., from modulation index 0.577 to 0.622. This paper reports 8 possible ways to realize the optimal strategy in one part of the OVM region and 2 possible ways in another part of OVM region. Each of these ways lead to different PWM techniques which have different current ripple and flux ripple performances. These performance comparisons are not explored in this paper and considered as future work. Finally, an optimal strategy has been identified which can be implemented per 3ϕ inverter basis without involving complex 6ϕ transformation. This technique uses 2 large, 1 medium and 2 small active vectors of $\alpha - \beta$ in one part of OVM and 2 large, 1 medium vectors in another part. With this strategy, the optimal solution is validated through experiments on laboratory scale hardware prototype and simulations in Matlab at 3.5 kW.

References

[1] F. Barrero and M. J. Duran, "Recent advances in the design, modeling, and control of multiphase machines—part i," *IEEE Transactions on Industrial Electronics*, vol. 63, no. 1, pp. 449–458, 2015.

[2] E. Levi, "Advances in converter control and innovative exploitation of additional degrees of freedom for multiphase machines," *IEEE Transactions on Industrial Electronics*, vol. 63, no. 1, pp. 433–448, 2015.

[3] Y. Zhao and T. A. Lipo, "Space vector pwm control of dual three-phase induction machine using vector space decomposition," *IEEE Transactions on industry applications*, vol. 31, no. 5, pp. 1100–1109, 1995.

[4] D. Hadiouche, L. Baghli, and A. Rezzoug, "Space-vector pwm techniques for dual three-phase ac machine: analysis, performance evaluation, and dsp implementation," *IEEE Transactions on Industry Applications*, vol. 42, no. 4, pp. 1112–1122, 2006.

[5] K. Marouani, L. Baghli, D. Hadiouche, A. Kheloui, and A. Rezzoug, "A new pwm strategy based on a 24-sector vector space decomposition for a six-phase vsi-fed dual stator induction motor," *IEEE Transactions on Industrial Electronics*, vol. 55, no. 5, pp. 1910–1920, 2008.

[6] C. Zhou, G. Yang, and J. Su, "Pwm strategy with minimum harmonic distortion for dual three-phase permanent-magnet synchronous motor drives operating in the overmodulation region," *IEEE Transactions on Power Electronics*, vol. 31, no. 2, pp. 1367–1380, 2016.

[7] J. Prieto, E. Levi, F. Barrero, and S. Toral, "Output current ripple analysis for asymmetrical six-phase drives using double zero-sequence injection pwm," pp. 3692–3697, 2011.

[8] C. Wang, K. Wang, and X. You, "Research on synchronized svpwm strategies under low switching frequency for six-phase vsi-fed asymmetrical dual stator induction machine," *IEEE Transactions on Industrial Electronics*, vol. 63, no. 11, pp. 6767–6776, 2016.

[9] J. Prieto, J. A. Riveros, and B. Bogado, "Continuous and discontinuous svpwm 2l+ 2m for asymmetrical dual three-phase drives," pp. 1–6, 2017.

[10] H. Eldeeb, C. Hackl, M. Abdelrahem, and A. S. Abdel-Khalik, "A unified svpwm realization for minimizing circulating currents of dual three phase machines," in *2017 IEEE 12th International Conference on Power Electronics and Drive Systems (PEDS)*, pp. 925–931. IEEE, 2017.

[11] A. Bakhshai, G. Joos, and H. Jin, "Space vector pwm control of a split-phase induction machine using the vector classification technique," in *Applied Power Electronics Conference and Exposition, 1998. APEC'98. Conference Proceedings 1998., Thirteenth Annual*, vol. 2, pp. 802–808. IEEE, 1998.

[12] R. Bojoi, A. Tenconi, F. Profumo, G. Griva, and D. Martinello, "Complete analysis and comparative study of digital modulation techniques for dual three-phase ac motor drives," in *Power Electronics Specialists Conference, 2002. pesc 02. 2002 IEEE 33rd Annual*, vol. 2, pp. 851–857. IEEE, 2002.

[13] K. Gopakumar, V. Ranganthan, and S. Bhat, "Split-phase induction motor operation from pwm voltage source inverter," *IEEE Transactions on Industry Applications*, vol. 29, no. 5, pp. 927–932, 1993.

[14] M. J. Duran, J. Prieto, and F. Barrero, "Space vector pwm with reduced common-mode voltage for five-phase induction motor drives operating in overmodulation zone," *IEEE Transactions on Power Electronics*, vol. 28, no. 8, pp. 4030–4040, 2013.

[15] G. Carrasco and C. A. Silva, "Space vector pwm method for five-phase two-level vsi with minimum harmonic injection in the overmodulation region," *IEEE Transactions on Industrial Electronics*, vol. 60, no. 5, pp. 2042–2053, 2013.

[16] A. Iqbal and E. Levi, "Space vector modulation schemes for a five-phase voltage source inverter," in *Power Electronics and Applications, 2005 European Conference on*, pp. 12–pp. IEEE, 2005.

[17] J. Prieto, F. Barrero, M. J. Durán, S. T. Marín, and M. A. Perales, "Svm procedure for n-phase vsi with low harmonic distortion in the overmodulation region," *IEEE Transactions on Industrial Electronics*, vol. 61, no. 1, pp. 92–97, 2014.

[18] T. Komrska, T. Glasberger, and Z. Peroutka, "Universal pwm modulator for multiphase drives with a minimum infinity-norm approach," *IEEE Transactions on Industrial Electronics*, vol. 63, no. 10, pp. 5979–5987, 2016.

[19] D. Yazdani, S. A. Khajehoddin, A. Bakhshai, and G. Joos, "Full utilization of the inverter in split-phase drives by means of a dual three-phase space vector classification algorithm," *IEEE Transactions on Industrial Electronics*, vol. 56, no. 1, pp. 120–129, 2009.

[20] J. Holtz, W. Lotzkat, and A. M. Khambadkone, "On continuous control of pwm inverters in the overmodulation range including the six-step mode," *IEEE Transactions on Power Electronics*, vol. 8, no. 4, pp. 546–553, 1993.

[21] H. S. Che, E. Levi, M. Jones, W.-P. Hew, and N. A. Rahim, "Current control methods for an asymmetrical six-phase induction motor drive," *IEEE Transactions on Power Electronics*, vol. 29, no. 1, pp. 407–417, 2013.

Sayan Paul received the B.Tech. degree from the National Institute of Technology, Durgapur, India in 2014; the M.Sc. (Engg.) degree from Indian Institute of Science, Bangalore, India in 2018, both in electrical engineering. He is currently pursuing the Ph.D. degree at the Electrical Engineering Department, Indian Institute of Science, Bangalore, India. His research interests include PWM techniques, modeling and control of multiphase drives, multi-level converters.

Kaushik Basu (S'07, M'13, SM'17) received the BE. degree from the Bengal Engineering and Science University, Shibpore, India, in 2003, the M.S. degree in electrical engineering from the Indian Institute of Science, Bangalore, India, in 2005, and the Ph.D. degree in electrical engineering from the University of Minnesota, Minneapolis, in 2012, respectively. He was a Design Engineer with Cold Watt India in 2006 and an Electronics and Control Engineer with Dynapower Corporation USA from 2013-15. Currently he is an Assistant Professor, in the Department of Electrical Engineering in Indian Institute of Science. He has been an author and coauthor of several technical papers published in peer reviewed journals and conferences. His research interests include various aspects of the general area of Power Electronics. He is the founding chair of both IEEE PELS and IES Bangalore Chapter.